Ice adhesion behavior of heterogeneous bituminous surfaces

F. Tarpoudi Baheri[a,b], L. D. Poulikakos[b], D. Poulikakos[a,1], T. M. Schutzius[c,2]

[a]Laboratory of Thermodynamics in Emerging Technologies, Department of Mechanical and Process Engineering, ETH Zurich, Sonneggstrasse 3, CH-8092 Zurich, Switzerland.

[b] Empa, Swiss Federal Laboratories for Materials Science and Technology, Überlandstrasse 129, 8600 Dübendorf, Switzerland

[c] Laboratory for Multiphase Thermofluidics and Surface Nanoengineering, Department of Mechanical and Process Engineering, ETH Zurich, Sonneggstrasse 3, ML J 27.2, CH-8092 Zurich, Switzerland

This document is the accepted manuscript version of the following article:
Tarpoudi Baheri, F., Poulikakos, L. D., Poulikakos, D., & Schutzius, T. M. (2021). Ice adhesion behavior of heterogeneous bituminous surfaces. Cold Regions Science and Technology, 192, 103405 (12 pp.). https://doi.org/10.1016/j.coldregions.2021.103405

[1] To whom correspondence should be addressed: Prof. Dimos Poulikakos, ETH Zurich, Laboratory of Thermodynamics in Emerging Technologies, Sonneggstrasse 3, ML J 36, CH-8092 Zurich, Switzerland. Phone: +41 44 632 27 38; Fax: +41 44 632 11 76; E-mail: dpoulikakos@ethz.ch;

[2] To whom correspondence should be addressed: Prof. Thomas M. Schutzius, ETH Zurich, Laboratory for Mulitphase Thermofluidics and Surface Nanoengineering, Sonneggstrasse 3, ML J 27.2, CH-8092 Zurich, Switzerland; Phone: +41 44 632 46 04; E-mail: thomschu@ethz.ch

Abstract

The phenomenon of icing, and the derived processes for its mitigation, are of great importance in many applications, ranging from transportation and energy to food and refrigeration. This phenomenon has been studied mostly with respect to its manifestation on rigid, homogeneous surfaces, with soft materials being the topic of more recent investigations. Although, icing often occurs on substrates that are chemically and mechanically heterogeneous, e.g., widely used asphalt concrete, which consists of rigid aggregates embedded in soft bitumen, to date, ice adhesion behavior on such substrates needs to be better understood. Here, we study ice adhesion stresses—the stresses necessary to remove ice—of ice blocks on heterogeneous materials, juxtaposing the behavior of the two main constituents of asphalt concrete, the rigid aggregates (modeled by Macor®) and bitumen, to the behavior of bitumen-Macor® composites. We show that the ice adhesion shear stress on Macor® is almost twice as large as that on bitumen, whereas the ice adhesion normal stress and the normal and shear components of composite stress are in a similar range. We synthesize composite substrates that consist of bitumen stripes on Macor® and find that increasing bitumen width leads to lower ice adhesion stress, while the stripe direction with respect to the applied force direction has a minor effect. Based on our findings, we then coat the most ice-adhesive component (Macor®) with a thin superhydrophobic coating and show that this can reduce ice adhesion stress on the heterogeneous substrates. We also find that for ice formed half on bitumen and half on Macor®, if Macor® is first and bitumen second with respect to the applied force direction (material order), then the measured ice adhesion stress is less compared to the reverse case in material order.

Keywords: ice adhesion, icephobic asphalt, heterogeneous surfaces, bituminous surfaces, road icing

Introduction

Despite its common manifestation on roads, roofs, terraces, and sidewalks in cold climates, the fundamental issue of surface icing—and passive methods to prevent it and facilitate its removal—is not well understood. This includes condensation freezing on roads and, consequentially, attempting to prevent or delay ice formation, as well as investigating facile removal principles of frozen or snow-covered pavements, leading to the introduction of methods to reduce the stress needed to remove ice (termed here as ice adhesion stress) and facilitate ice removal. Road surfaces consist of two main components: Rigid aggregates (gravel), which are held together by a soft viscoelastic bituminous binder. They have drastically different wettability and stiffness properties, causing road surfaces to be both chemically and mechanically heterogeneous.

To date, research on ice adhesion mechanisms has focused on rigid materials (Kulinich and Farzaneh, 2009; Matsumoto and Kobayashi, 2007; Rønneberg et al., 2020; Schutzius et al., 2015; Work and Lian, 2018), proposing textured low-surface energy coatings possessing low ice adhesion stress (Meuler et al., 2010). Liquid-infused (i.e., lubricated) surface technology has attempted to take advantage of embedded liquid interface properties in solid structures to reduce ice adhesion stresses (Baker et al., 1962; Kim et al., 2012; Metya and Singh, 2019; Wilson et al., 2013). It is shown that the rigid phase arrangement and area fraction of the liquid-infused surface can control ice adhesion by governing local conductive heat transfer, ice-substrate

interaction, and locally cracking initiation of the iced interface (Metya and Singh, 2019; Wilson et al., 2013). Recently, the impact of substrate compliance on ice adhesion stress has attracted researchers' attention, and a number of studies have been undertaken on this topic (Beemer et al., 2016; Chaudhury and Kim, 2007; Chung et al., 2006; Chung and Chaudhury, 2005; Golovin et al., 2019; Petit and Bonaccurso, 2014; Vasileiou et al., 2017). Petit *et. al.* have shown that substrate compliance does not have a significant role on freezing initiation time while later the substrate deformation influences interfacial area and consequently freezing process is faster on softer substrates (Petit and Bonaccurso, 2014). Applied force on frozen interfaces can form surface instabilities and fringes, depending on the soft substrate thickness and the neighboring material properties, whether soft or rigid (Chung et al., 2006; Chung and Chaudhury, 2005). It has been shown that a rigid object on a compliant substrate slides in shear mode unless the developing normal force (at the location of the applied force) reaches a critical value and detaches the interfaces of the rigid object and soft substrate (Chaudhury and Kim, 2007). Despite the brittle ice removal from rigid materials, it is shown that ice detaches from soft surfaces in a dynamic stick-slip motion i.e., intermittent movement with recurring cycles of stationary and sliding phases (Beemer et al., 2016). Furthermore, for long enough ice blocks, ice adhesion could become independent of the ice area which results in very low ice adhesion stresses for large area ice-soft material interfaces (Golovin et al., 2019).

While the behavior of ice on homogeneous surfaces is understood to a degree, the fundamentals of ice formation and adhesion on heterogeneous substrates—for both wettability and stiffness—are not, and relatively few studies have been conducted on this topic (Irajizad et al., 2019a; Liu et al., 2017; Sivakumar et al., 2021). Liu *et al.* showed that substrate hydrophobic-

hydrophilic boundaries can block the ice-substrate front and alter the ice growth mode transition when the wettability of the solid substrate changes (Liu et al., 2017). Irajizad *et al.* measured ice adhesion stresses on heterogeneous materials —a low shear modulus material dispersed in a high shear modulus matrix— and showed that stress mismatch of ice interface with heterogeneous substrate can reduce ice adhesion stress (Irajizad et al., 2019a). Once a minimal force is applied (resulting in approximately 1 KPa), ice detaches from the low shear modulus material phase and forms cavities at the interface of the substrate material and ice, leading to a stress concentration around the cavity and inducing crack and cavity growth and fracture of interfaces (Irajizad et al., 2019a). Experiments performed on patterned rigid-soft substrates of aluminum-polyurethane have shown that by increasing the area fraction percentage of the softer component (stripes from 2mm width to 10 mm, respecting 0% to 77% for 26 mm square samples), the ice adhesion is reduced independently of the substrate heterogeneity direction (stripes in the aluminum filled of the softer polyurethane phase) on the anisotropic substrate (Sivakumar et al., 2021).

Several ice adhesion studies have been conducted specifically on road surfaces, mostly focusing on practical applications (Arabzadeh et al., 2017, 2016; Chen et al., 2018b, 2018a; Dan et al., 2014; Gao et al., 2018; Peng et al., 2018; Penn and Meyerson, 1992; Xia et al., 2020). It is shown that regardless of the bulk water or ambient conditions a layer of small, bubble-free ice crystals nucleate on the pavement surface once its temperature drops below subzero (Penn and Meyerson, 1992). However, this layer is strong and well adhered, but if the nucleation could be prevented using either salt or changing the substrate surface energy, ice adhesion would be weaker due to larger ice crystals that form from the bulk water and entrapped bubbles (Penn and Meyerson, 1992). Peng *et al.* showed that replacing asphalt concrete fillers with anti-freezing salt-

based components and fumed silica-based coating can delay freezing and significantly reduce the ice adhesion stress (Peng et al., 2018). Arabzadeh *et al.* showed that spraying superhydrophobic coatings on asphalt surfaces can also reduce ice adhesion stress (Arabzadeh et al., 2017, 2016). By lowering the substrate asphalt concrete temperature from 0 °C to -10 °C, cohesive failure in ice becomes dominant compared to adhesive failure at the interface (Chen et al., 2018b). In large-scale asphalt concrete samples, Dan *et al.* found that the normal-tension ice adhesion depends logarithmically on the ice temperature, whereas in the case of the shear stress, a linear relation was exhibited (Dan et al., 2014).

In this study, we investigate the fundamentals of ice adhesion stress on heterogeneous bituminous surfaces at smaller sub-centimeter scales. To this end, at sample surface temperature of T2 = -19.5 ± 0.5 °C, the impact of substrate mechanical and chemical heterogeneity on ice adhesion stress is studied by juxtaposing soft viscoelastic bitumen next to rigid glass-ceramic aggregates that we model by Macor®. We synthesize heterogeneous substrates that consist of bitumen stripes on Macor® and find that increasing stripe width—for the same ice block size—leads to lower ice adhesion stress. We also find that the stripe direction with respect to the applied force direction does not have a pronounced effect on ice adhesion stress. Based on these findings, we then focus on modifying Macor®, the most adhesive component of the heterogeneous substrate, and to this end, we exploit an up-scalable, superhydrophobic, durable coating technique. We confirm that a superhydrophobic coating can significantly reduce the ice adhesion stress on Macor®. We also find that for ice blocks that are half on the bitumen stripe and half on Macor® (also superhydrophobic Macor®), if the rigid Macor® is first and softer bitumen second with respect to the applied force direction, then the measured ice adhesion

stress is less compared to the reverse case. Our findings add to necessary fundamental knowledge contributing to the design of bituminous surfaces with facile ice removal behavior, paves the path for further studies in the future.

Methods and Material Studied

Materials

Figure 1a shows a schematic of an ice block on a heterogeneous bituminous surface consisting of rigid Macor® (white) and soft bitumen (black), with the applied force for the removal of this block shown with the red arrow. The material used for the soft component was virgin bitumen Q8 70/100 with penetration grade 70/100, density 1.029 g/cm^3 of Middle Eastern origin with a medium softness range of 82 (0.1 mm) needle penetration (EN 1426), and softening temperature (EN 1427) of 45.8 °C, and dynamic viscosity of 163 Pa-s at 60 °C. For this type of bitumen, differential scanning calorimetry (DSC) results indicated that its glass transition temperature is ca. -20 °C and that it has a melting peak at ca. 28 °C. The reported SARA (saturates, aromatics, resins, and asphaltene) factions of this bitumen type are 3.8, 59.6, 22.2, and 14.6 %, respectively (Fischer et al., 2014; Soenen et al., 2014). SARA analysis is an operational method to separate the bitumen into its characteristic finite fractions according to the polarity, molar mass and aromatic content of the molecules (Yu et al., 2015). Figure 1b, and c show the significant mechanical and wetting behavior differences, relevant to ice adhesion, between the employed bitumen and Macor®. Bitumen is a temperature- and frequency-dependent viscoelastic material with a complex modulus, *G*, of 0.15 MPa at 20 °C and 81 MPa at -10 °C under 0.1 Hz, 10 % strain, Figure 1b (see also Figure A1). Aggregates have random shapes and uncontrolled surface

properties; therefore, we used Macor® as a representative material for asphalt concrete aggregates. Macor® has a complex modulus of 25.5 GPa over the experimental temperature range of this study, Figure 1b. The surface of bitumen is generally hydrophobic with an advancing contact angle of > 110° and a receding contact angle of ca. 75°, Figure 1c. On the other hand, Macor® is superhydrophilic and has a receding angle of < 5°, Figure 1c.

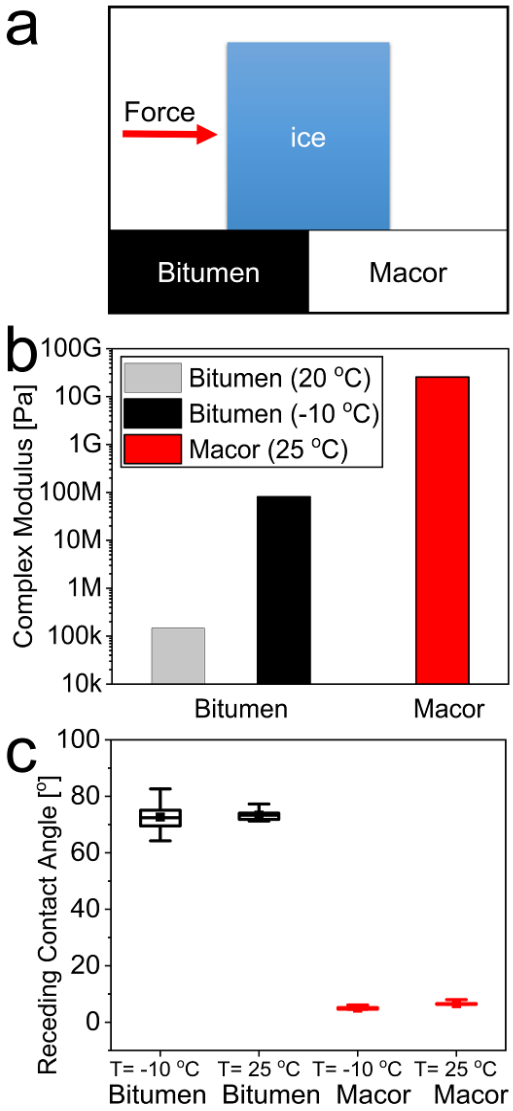

Figure 1 Ice adhesion on road-like materials at subzero temperatures. a) General schematic of ice formation on heterogeneous road-like surfaces. b) Complex modulus of bitumen at 20 °C and -10 °C at 0.1 Hz versus reported complex modulus of Macor®

material at 25 °C ("MACOR® Machinable Glass Ceramic For Industrial Applications," 2021). c) Receding contact angle of a water droplet on bitumen surface and Macor® at two sample temperatures of 25 °C and -10 °C and environmental condition of *RH* < 1% at 24 ± 1 °C.

Such high contact angle hysteresis on bitumen could be due to surface tension driven substrate deformation—due to its softness at room temperature—at the triple contact line, as has been shown for other soft substrates (Carré et al., 1996; Gerber et al., 2019; Lee et al., 2016). Furthermore, previous work has shown that the surface of bitumen is complex, possessing heterogeneous surface chemistry and intrinsic roughness that potentially can affect contact angle hysteresis (Tarpoudi Baheri et al., 2020). Macor®, on the other hand, is a machinable glass-ceramic with similar properties to common aggregates such as limestone, basalt, and sandstone, and its hydrophilic property is to be expected, Table 1.

Table 1 **Properties of commonly used *asphalt concrete aggregates and Macor® material* at 25 °C** ("MACOR® Machinable Glass Ceramic For Industrial Applications," 2021). Where values of, thermal conductivity (K), specific heat (C_P), density (ρ), apparent contact angle θ^***,** and complex modulus (G) are reported.

	Thermal conductivity K (W.m^{-1}.K^{-1})	**Specific heat C_P (J.kg^{-1}.K^{-1})**	**Density ρ(kg.m^{-3})**	**Contact angle θ^* (deg)**	**Complex modulus *G* (GPa)**
Macor®	1.46	790	2520	Advancing: 28 ± 2 Receding: < 5	25.5
Basalt	1.7	840	2400-3100	74 ± 5	50
Limestone	1.26-3.0	909	2700	-	3-27

Sandstone	1.7-3.0	710-900	2850	-	10-20

Measurements shows that Macor® has microscale surface features with an average root-mean-square (RMS) surface roughness of 0.34 ± 0.04 µm (see Figure A2 and Figure A3) whereas previous studies found that for aggregates used in pavement, including for cold regions applications, that the average RMS surface roughness was in the order of tens of micros (Gan, 2017; Perez et al., 2015; see also Table A1). Based on the above, one should anticipate differences, with respect to ice adhesion, between the behavior of such a composite material and the case where the surface consists one of those materials, acting alone.

Substrates and Coatings

To fabricate thin virgin bitumen coatings on a Macor® substrate—and also to create thin stripes of bitumen in Macor® notches—we used a solvent casting approach. To prepare the bitumen solution, 1 g of virgin bitumen was diluted in 4 ml toluene (Sigma-Aldrich 99.8%) at room temperature (ca. 25 °C) and mixed using a shaker (Heidolph Multi Reax) at 2,000 rpm for 2 minutes. A drop of 150 µl virgin bitumen solution was then dispensed on Macor® disks (1 mm thick, 18 mm diameter). The solvent cast sample was left under a fume hood in ambient conditions until most of the toluene solvent evaporated, which was observed to occur within half an hour. Next, samples were heated on a hotplate at 115 °C for five minutes, above the bitumen softening temperature of 45.8 °C and the toluene boiling temperature of 111 °C, to ensure uniform and smooth surfaces. Thereafter, the samples were placed in a refrigerator for five minutes at 4 ± 2 °C to cool and solidify the bitumen coating layer. The final bitumen thickness was measured to be ≈ 225 µm (see also Figure A4a).

To create superhydrophobic surfaces on Macor®, we deposited polymer-nanoparticle dispersions onto it by spray coating following a previously published method (Schutzius et al., 2011). The coating thickness was ca. 25 µm (see also Figure A4b). To prepare the dispersion for spray, we first made two stock solutions and a nanoparticle suspension. The first stock solution consisted of 10 wt.% PVDF (polyvinylidene fluoride) in NMP (N-Methyl-2-pyrrolidone) and was generated by adding PVDF to NMP and then mixing it slowly for 5 hours at 40 °C. The second stock solution consisted of 10 wt.% PMMA (poly(methyl methacrylate)) in acetone and was generated by combining PMMA beads with acetone and mixing it at 1200 rpm for 8 hours. The nanoparticle suspension consisted of 10 wt.% hydrophobic fumed silica (HFS; Aerosil R 8200, Evonik Industries) in acetone and was created by combining HFS and acetone and probe sonicating it for 30 seconds (130 W, 3 mm probe, 50% amplitude, 20 kHz frequency, Sonics Vibracell, VCX-130). One portion of each of the two solutions and ten portions of suspension were then combined and diluted with additional ten portion of acetone, resulting in a final 12 g mixture (for 0.5 g portions) can approximately coat an area of 25 cm^2. To create stripes of bitumen on Macor®, 200 µm deep notches were cut into the Macor® surface, with widths of either 0.5, 1, or 1.8 mm, and then they were filled with the bitumen-toluene solution (~22 wt.%, 1 gr bitumen in 4 µl toluene). The ice mold that we use to measure ice adhesion is a tube that has an inner diameter (ID) of 1.8 mm, so these bitumen stripe widths of 0.5, 1, and 1.8 mm correspond to ice-bitumen contact area fractions of ϕ = 35%, 67%, and 100% (experiments described in detail later). We used pure Macor® surfaces (ϕ = 0% bitumen-ice contact area) as control samples.

Characterization

We used a commercial goniometer (OCA35, DataPhysics Instruments GmbH) to perform contact angle measurements in sessile mode contact angle at 0.5 µl/s dosing rate with final droplet volume of 10 µl. A homemade environmental chamber was installed on the goniometer stage for contact angle measurements in order to control sample temperature and environment relative humidity (*RH*) conditions (see Figure A5). The inlet nitrogen stream at room temperature provided *RH*< 1%. The contact angle measurements were conducted at two sample temperatures of 25 °C and -10 °C, controlled by a thermoelectric element. Commercial software was used for contact angle post-processing (DataPhysics Instruments GmbH).

We performed ice adhesion in three modes of *pure shear stress* (applied force parallel and tangential to the substrate), *combined stress* (applied force at a finite height from the substrate and parallel to it), and *normal-tension stress* (force perpendicular to the substrate). The ice adhesion setup comprised four main elements (see Figure A6a, and b). A commercial cryogenic system was used as the cooling stage to cool the substrates to subzero temperatures (BSC 196 from Linkam Scientific Instruments Ltd.). The stage temperature was set to -24.5 °C, and the surface temperature was measured T2 = -19.5 ± 0.5 °C by a T-type thermocouple. A copper plate was designed and installed on the cold stage for mounting and holding samples firmly. At least 20 minutes of conditioning time was considered after cooling the stage from room condition to the target temperature at -20 °C/min to ensure the water column was frozen on the sample. An environmental chamber was built from transparent Plexiglas® and mounted on top of the cryogenic stage to control humidity and prevent condensation and frosting on the sample. Inlet N_2 gas guarantees dry environmental condensation to prevent frost formation on the surfaces.

Over the conditioning time before conducting the ice adhesion stress measurement experiments, environmental conditions stabilize at T1 = 13 ± 1 °C and *RH* < 1% and environmental temperature of 24 ± 1 °C.

A force sensor (Mark-10 model M5-5) was connected to a rod in order to induce and measure the ice adhesion force for a given ice-substrate contact area. An opening at the chamber wall was used as an access point for the force sensor rod. A pointed head was installed on the rod for the pure shear and combined stress ice adhesion tests to push 9 mm tall ice mold made of hard plastic (polystyrene) cylinders with an inner diameter of D_{i} = 1.8 mm and an outer diameter D_o = 3 mm. Initially, the empty ice molds were gently placed on the sample surface and then filled with deionized water up to 8 mm in height from the bottom. The height of the tip of the rod from the sample surface (*h*) was set to zero for the *pure shear mode* (Figure A6a). For combined stress, a force was applied parallel to the substrate surface at the center-of-mass of the ice (*h* = 4 mm). For the normal-tension mode, a triangular ring was attached to the same size ice molds. The force rod was mounted on top of the ice cylinder and connected to it by a hook, and the force was applied away from and normal to the substrate surface.

The force sensor was installed on linear stage (NRT150/M, Thorlabs, Inc.), and the height (*h*) was adjusted by a lab jack (L490/M, Thorlabs, Inc.), according to the required experimental modes. All ice adhesion experiments were conducted by induced force from a rod starting from a stationary mode with an acceleration of a = 0.01 mm/s^2, far enough to reach the constant velocity of V = 0.1 mm/s steady-state velocity condition at contact. This velocity was selected based on commonly reported and recommended values in other similar ice adhesion experiments (Irajizad et al., 2019b; Meuler et al., 2010; Wang et al., 2014).

Samples were placed in configuration to accommodate two bitumen stripe directions, resulting in a perpendicular force and the other to result in a parallel force with respect to the notch. For the composite bitumen-Macor® samples, the circular ice mold was placed on the bitumen stripe so that the stripe was in the middle of the ice cross-sectional area. Despite the directional independence of samples in the normal-tension ice adhesion mode, these samples were installed in a perpendicular direction as defined before (Figure A8a). To compare mean value differences between each set of data for different ice adhesion tests on heterogeneous materials, we conducted a statistical two-sampled, two-sided Student's t-test and determined the probability (*P*) associated with a Student's paired-test.

In the configuration where the ice mold cross-sectional area was placed on the bitumen-Macor® boundary where the bitumen stripe width was 1.8 mm so that half of the ice area was in contact with the bitumen and the other half was in contact with the Macor® ceramic (Figure A8b). For two ice adhesion modes of pure shear stress and combined stress, the impact of the material order was examined with respect to the applied force, which was parallel to the substrate surface.

Results and Analysis

First, we show the results of the ice adhesion experiments on homogeneous Macor® and virgin bitumen. Figure 2a-c depicts a schematic drawing of the ice adhesion experimental setup in three different modes: pure shear stress, combined stress, and normal-tension stress, respectively. Figure 2d-f show plots of the experimentally measured force vs. time in these three different modes on bitumen and Macor® substrates; the maximum magnitude of the force required to remove ice from the substrate, F^*, measured during these experiments were used to

calculate the ice adhesion stress along with the ice-substrate contact area. The combined stress mode has a lower *F** due to the torque generated by force acting at the bottom corner of the mold. Figure 2g-i shows ice adhesion stresses based on *F** on bitumen and Macor®, for the three modes of pure shear (τ^*_{shear},), combined stress (τ^*_{cs}, and σ^*_{cs},), and normal-tension ($\sigma^*_{\mathrm{normal}}$). We calculate the pure shear ice adhesion stress by $\tau^*_{\mathrm{shear}} = 4F^*/(\pi D_{\mathrm{i}}^2)$, the combined ice adhesion stress by $\tau^*_{\mathrm{cs}} = 4F^*/(\pi D_{\mathrm{i}}^2)$ and $\sigma^*_{\mathrm{cs}} = 8hF^*/(\pi D_{\mathrm{i}}^3)$, and the normal ice adhesion stress by $\sigma^*_{\mathrm{normal}} = -4F^*/(\pi D_{\mathrm{i}}^2)$.

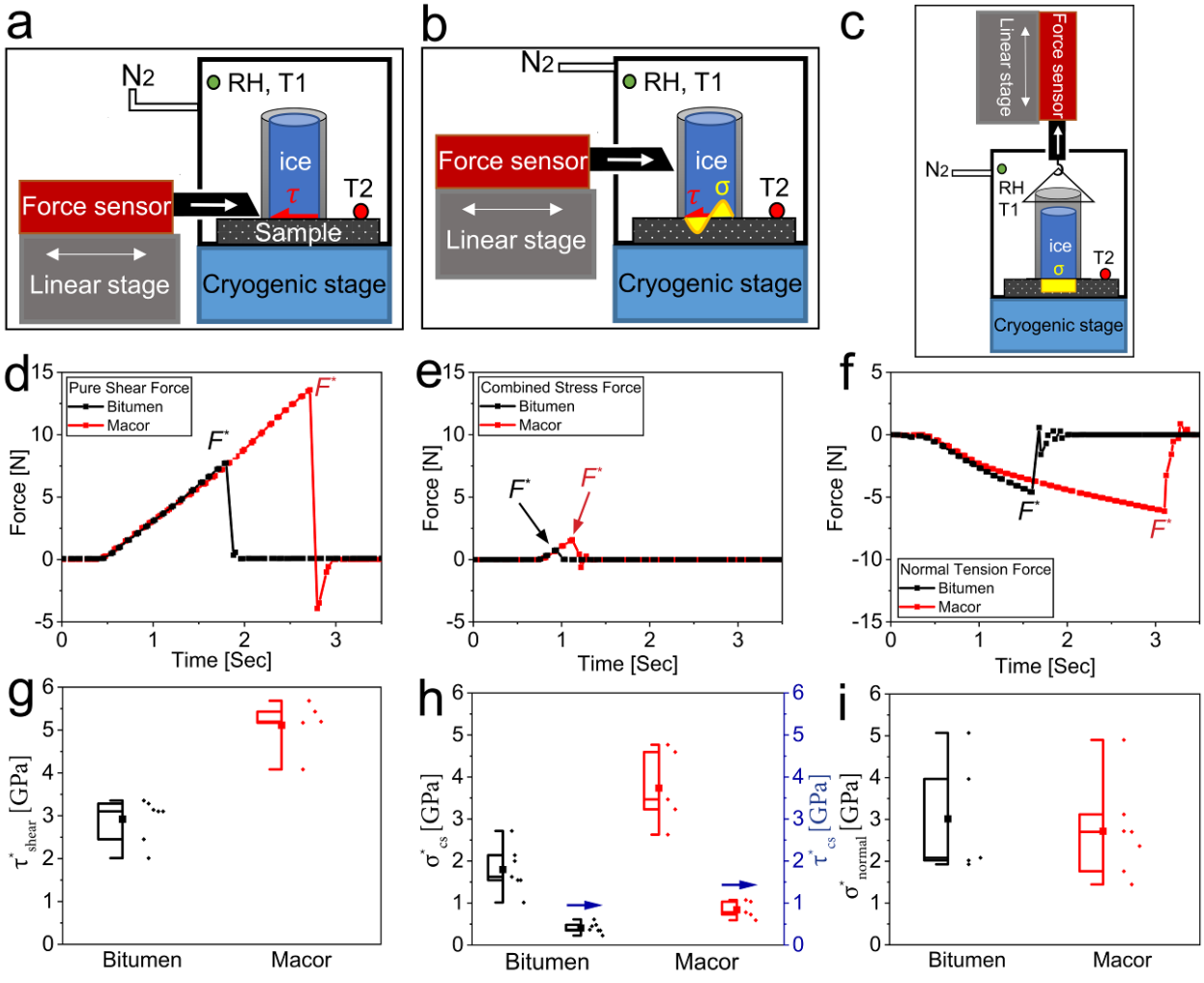

Figure 2 Ice adhesion modes on heterogeneous bitumen. Schematic drawing of experimental modes to measure a) pure shear stress b) combined stress, and c) normal-tension stress. Examples of experimentally measured force curves vs. time for d) pure

shear stress, e) combined stress, and f) normal-tension stress ice adhesion modes. Calculated stresses based on absolute peak force *F**defined in (d) (e) or (f) are plotted in the box plot (left) and data points (right) for three modes of g) pure shear (τ^*_{shear}), h) combined stresses (σ^*_{cs} and τ^*_{cs}), and i) normal-tension ($\sigma^*_{\mathrm{normal}}$) plotted for the absolute tensile force value. Each data point represents an experiment of ice adhesion stress measurement.

*F** was higher on Macor® in all investigated modes compared to bitumen. Also, such force vs. time plots are consistent with a brittle breakage behavior, as the force values drop rapidly after the peak, especially for the pure shear and normal-tension modes. For the combined stress ice adhesion measurements, σ^*_{cs} is significantly greater than τ^*_{cs}, indicating that normal stresses dominate. This is due to the mathematical correlation $\sigma^*_{\mathrm{cs}}/\tau^*_{\mathrm{cs}} = 2h/D_i$ depending on of *h* and D_i values. The value of τ^*_{shear} as well as τ^*_{cs} and σ^*_{cs} on Macor® are approximately twice the corresponding values on the bitumen substrate alone (Figure 2g, and h). From this, we see that ice adheres stronger to Macor® relative to bitumen. In contrast, the value of $\sigma^*_{\mathrm{normal}}$ on bitumen and Macor® shows higher data scattering (Figure 2i). This can be explained by Kendall's theory describing removal of a rigid object from an elastomer in tensile mode. Based on this theory, the tensile modulus is three times higher than the shear modulus (Kendall, 1971; C. Wang et al., 2018). Here we assume that viscoelastic bitumen is primarily elastic in cold temperatures, which explains the fact that primarily tensile failure was seen.

Using heterogeneous bituminous surfaces that consist of a bitumen stripe on Macor®, Figure 3a shows plots of τ^*_{shear} vs. the bitumen-ice contact area fraction, ϕ. ϕ was varied by varying the stripe width while keeping the ice-substrate contact area the same. The direction of the bitumen stripe along its long length is perpendicular to the applied force for four bitumen-ice surface fractions (ϕ = 0%, 35%, 67%, and 100%). Figure 3b shows a plot of τ^*_{shear} vs. ϕ for the configuration where the stripe direction along its long length is parallel to the applied force

direction. Results of the probability (P), associated with a Student's paired T-test, with a two-tailed distribution, are shown for each pair of samples only when the difference between two groups is significant (i.e. $P < 0.05$) by red lines.

Figure 3c and Figure 3d shows plots of σ_{cs}^{*} and τ_{cs}^{*} vs. ϕ for the cases where the applied force—which is applied parallel to the substrate interface—is acting in a direction that is perpendicular and parallel to the bitumen stripe along its long direction, respectively. Figure 3e shows a plot of $\sigma_{\mathrm{normal}}^{*}$ vs. ϕ.

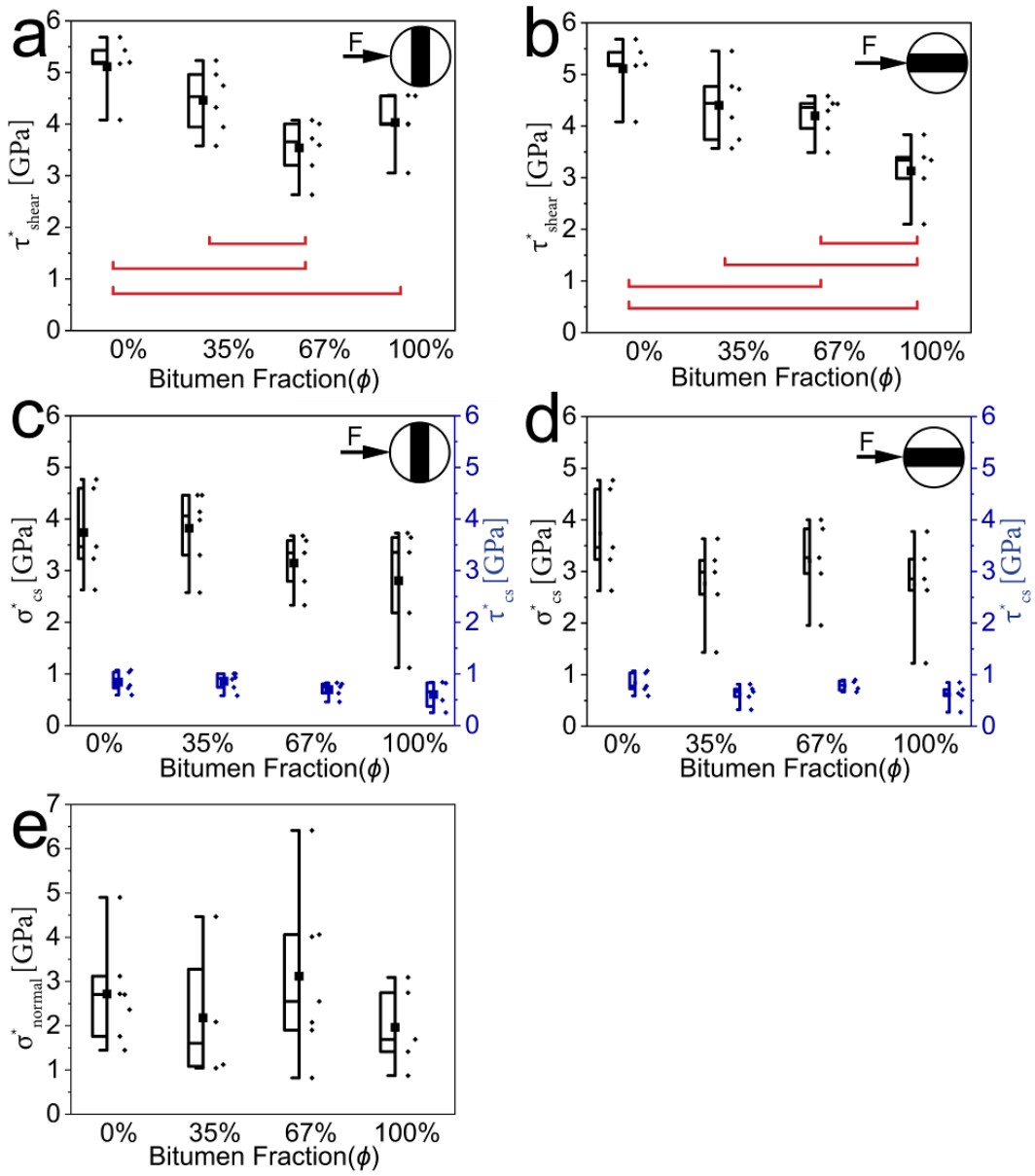

Figure 3 Impact of substrate heterogeneity and anisotropy on ice adhesion. Results are shown for four bitumen-ice area fractions of ϕ = 0% (i.e., pure Macor®), 35%, 67%, and 100%. Samples were installed in two selective stripe directions—defined as the direction along the long length of the stripe—namely, perpendicular and parallel to the applied force. Plots of τ^*_{shear} vs. ϕ for a) perpendicular and b) parallel applied force directions; results of probability associated with a Student's paired T-test, with a two-tailed distribution, are shown by red lines only for each pair of samples only when the difference between two groups is significant (i.e. $P < 0.05$). Plots of σ^*_{cs} and τ^*_{cs} vs. ϕ for c) perpendicular and d) parallel applied force directions. e) Plot of $\sigma^*_{\mathrm{normal}}$ vs. ϕ, and such measurements are neutral to the direction of the stripe with respect to the applied force direction; but samples were installed in similar perpendicular directions as panels (a) and (c).

When bitumen is ϕ = 0%, this means that the substrate is pure Macor®, and such substrates have the highest values of τ^*_{shear} of the four surface bitumen fractions studied. The lowest value of τ^*_{shear} was measured in the case of ϕ = 67% (Figure 3a). In the case of an applied parallel force to the bitumen stripe (Figure 3b), τ^*_{shear} correlates well with ϕ. Similar to the combined stress results in Figure 3c-d, the values of $\sigma^*_{\mathrm{normal}}$ in Figure 3e show a large spread. As mentioned before, in our experimental mode for the combined shear stress measurements, the value of σ^*_{cs} (magnitude) is larger than τ^*_{cs}. From the T-test comparison (Figure 3a, b), it is evident that ϕ has a marked impact on τ^*_{shear} but not on σ^*_{cs}, τ^*_{cs} , and $\sigma^*_{\mathrm{normal}}$.

Armed with an improved knowledge of ice adhesion stress on both homogeneous and composite samples, we can state that Macor® is the component with the highest values of τ^*_{shear} , σ^*_{cs}, τ^*_{cs} , and $\sigma^*_{\mathrm{normal}}$. To reduce its adhesion to ice, we deposited a previously developed superhydrophobic coating (Schutzius et al., 2011) onto the Macor® surface. Micrographs of pure Macor® (Figure 4a) and the superhydrophobic coated Macor® (Figure 4b; SHM) reveal that the coating is uniform. SHM was measured to have a receding contact angle of > 150° at room condition (Figure 4c) with very small < 1° contact angle hysteresis. Even with care taken to keep environmental conditions dry, while cooling the substrate to -10 °C, condensation likely formed on the Macor® and SHM surface roughness, causing the receding contact angle to decrease. This is a result of the fact that the droplet is at ambient temperature and has a higher vapor pressure around the droplet (Mitridis et al., 2020). Using Macor® and SHM substrates, Figure 4d, Figure 4e, and Figure 4f show plots of τ^*_{shear} ; σ^*_{cs} and τ^*_{cs} ; and $\sigma^*_{\mathrm{normal}}$, respectively.

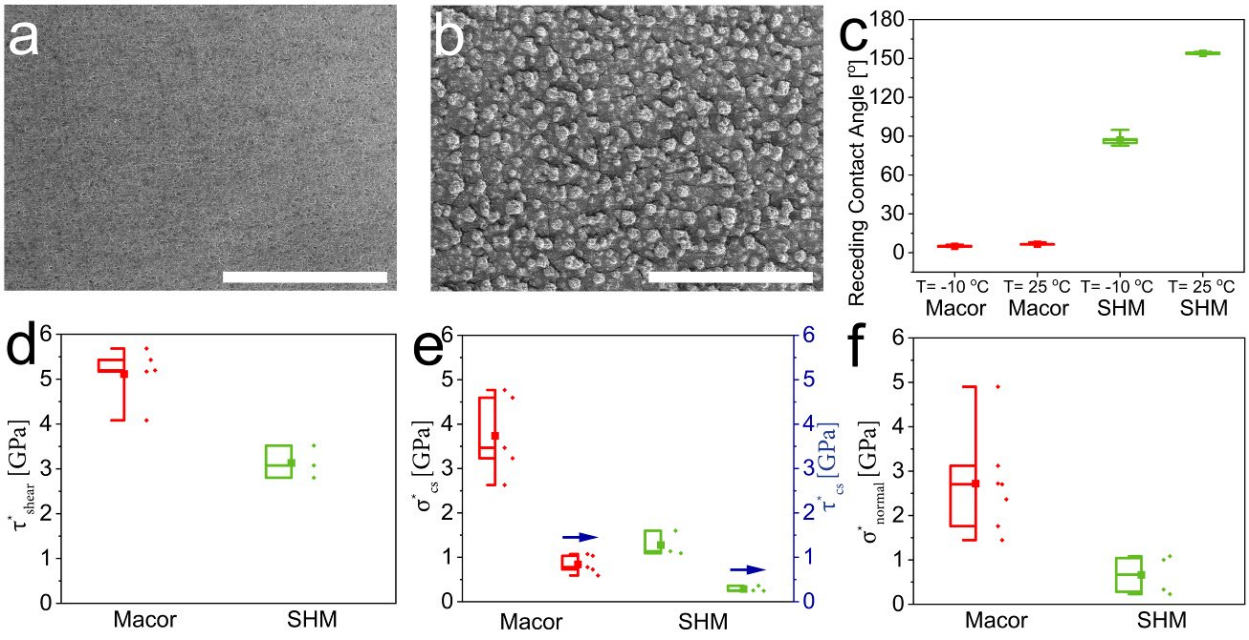

Figure 4 Reducing ice adhesion to Macor®. Micrographs of a) a pure Macor® surface and b) a Macor® substrate with a superhydrophobic coating (SHM). c) Receding contact angles of a water droplet on Macor® and SHM at two sample temperatures of 25 °C and -10 °C and environmental condition of *RH* < 1% at 24 ± 1 °C. Plots of ice adhesion stress on Macor and SHM: d) τ^*_{shear} , e), σ^*_{cs} and τ^*_{cs}, and f) $\sigma^*_{\mathrm{normal}}$. Scale bars: (a)-(b) 1 mm.

The wettability results show that the superhydrophobic behavior of this and any other similar coating depends on the environmental temperature and the relevant values of contact angles are not those of measurements in standard atmospheric conditions but those measured at the actual low-temperature experimental conditions (Figure 4c). Increasing the hydrophobicity of Macor® leads to a decrease in τ^*_{shear} , σ^*_{cs}, τ^*_{cs} , and $\sigma^*_{\mathrm{normal}}$ —by approximately half— compared to its initial value on untreated Macor® (Figure 4d-f). Several possible mechanisms contribute to reducing ice adhesion stress on hydrophobic surfaces. First, trapped air pockets in the surface topography of hydrophobic coatings provide weak mechanical bonding between ice and substrate (Shen et al., 2015). These cavities can behave as localized stress zones and make it easier to break the ice–substrate interface (N. Wang et al., 2018). Secondly, low surface energy coatings can reduce ice adhesion stress (Meuler et al., 2010). Furthermore, it is possible that a

portion of the superhydrophobic coating is actually removed during the ice detachment process, with the top layer of the coating acting as a sacrificial layer. From the practical aspects, on the one hand, using a superhydrophobic coating on pavements raises concerns of coating durability, and the reduced traction forces on the pavement due to surface chemical treatments that could negatively affect skid resistance. On the other hand, it is shown that mechanical hysteresis resulting from rubber tire deformation with pavement's rough surface topography can hold the required friction (Ahammed and Tighe, 2009; Arabzadeh et al., 2017, 2016; Kogbara et al., 2016).

Before discussing our results further, we reiterate our objective of increasing the intrinsic icephobicity of surfaces relevant to roads after understanding ice adhesion on heterogeneous bituminous surfaces with the main component elements of road surfaces (bitumen and gravel). The next consideration is the effect of the *material order* in the direction of applied force (that is, bitumen first or Macor® first) on ice adhesion stress. The ice contact areas on these materials are equal. Figure 5a shows a plot of τ^*_{shear} vs. the material order appearance with respect to the applied force direction for bitumen-Macor® and bitumen-SHM substrates. Figure 5b shows a plot of σ^*_{cs} and τ^*_{cs} vs. the material order appearance with respect to the applied force direction for bitumen-Macor® and bitumen-SHM substrates.

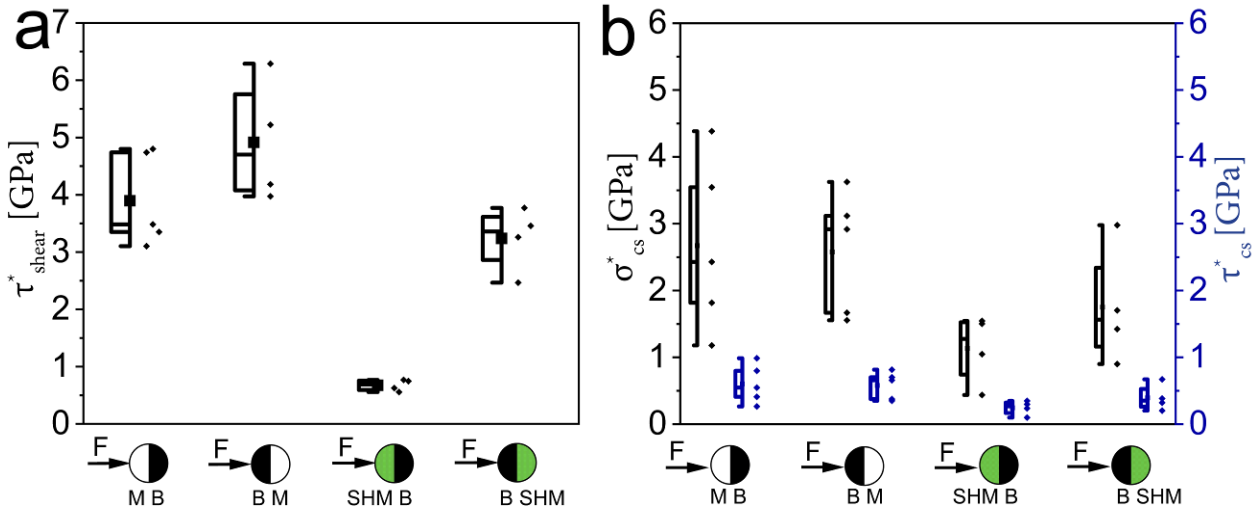

Figure 5 The role of material order on ice adhesion to heterogeneous bituminous surfaces. Ice adhesion on the boundary of compliant-rigid materials and impact of the material order for ice adhesion mode of a) τ^*_{shear} and b) σ^*_{cs} and τ^*_{cs}. The color code and abbreviations are black for bitumen (B), red for Macor® (M), and green for chemically coated superhydrophobic Macor® (SHM).

When the rigid Macor® (or SHM) is placed before the softer bitumen, τ^*_{shear} is lower than in the opposite case, Figure 5a. In both material order configurations, by making the Macor® superhydrophobic, the value of τ^*_{shear} decreases. Notably, lower τ^*_{shear} were recorded when synergy both parameters of the material order and Macor® surface coating. The lowest value of τ^*_{shear} was measured when the SHM was the first material to appear—relative to the applied force—followed by bitumen. In the case of the combined stress, the material order appearance relative to the applied stress direction has an effect on σ^*_{cs} and τ^*_{cs} , although both results are less pronounced compared to the pure shear stress case. Although σ^*_{cs} is larger than τ^*_{cs} , the trend remains similar, and the SHM-bitumen substrate shows a lower ice adhesion stress (Figure 5b).

The above behavior—where the ice adhesion stresses are lower when the rigid material appears first, and the softer material appears second relative to the applied force—can be explained by the interfacial interaction of ice with rigid and soft substrates. Soft materials, to an

extent, can deform by the stresses in any direction, while rigid materials cannot follow interfacial strains in contact with another solid body. The elasticity of a soft substrate can potentially prevent early micro-crack formation under small strains, and the existing cracks cannot connect and propagate along with the interface. The applied force hits the ice mold from a single point with a high-stress concentration at the location of force. Therefore, when the soft material appears first relative to the applied force, larger stresses on the soft material can be paid off by high strains and allow the rigid section also contributes to the carrying ice adhesion stress. When the rigid section is the first material, due to negligible strain, the stress cannot completely transmit, and the contribution of the soft section remains limited. Thereafter, the half area of the ice mold on the rigid section mainly takes the stresses, and when the stress reaches the critical point, the ice substrate detaches by lower applied forces.

Discussion and conclusions

This study investigated ice adhesion on heterogeneous (bitumen-Macor®) materials representative of elementary road surface composition in three modes: pure shear, combined stress, and normal-tension. We showed that Macor® yields the highest ice adhesion stresses compared to bitumen. Two parameters of the sample heterogeneity, namely, direction with respect to the applied force (perpendicular or parallel) and the bitumen fraction of the composite substrates mainly affect the pure shear mode adhesion. By increasing the bitumen fraction, the pure shear stress mode showed a decreasing trend. Moreover, it is shown that a superhydrophobic coating can reduce the ice adhesion stresses of rigid Macor® at low temperatures. Ice adhesion stresses of Macor® after surface treatment decrease to the same

range as for homogeneous bitumen alone and is half of the initial (before coating) value of pure Macor®. We also found that for ice formed half on the bitumen and half on Macor® (or Macor® made superhyrophobic), if Macor® is first and bitumen second (material order), with respect to the applied force direction, then the measured ice adhesion stress is less compared to the reverse case. This material order combined with the surface treatment modification reduced ice adhesion stresses further. In this case, the results were also lower than ice adhesion stress values for each component material.

The present basic results show concepts that can affect ice adhesion on surfaces relevant to road and other applications, where mechanical heterogeneity is present. Future studies can exploit such basic concepts on larger scale applications, aiding the development of surfaces with facile ice removal properties, while also complying with available guidelines and standards of mechanical performance, skid resistance, and environmental footprint.

Acknowledgments

This work was supported by the Swiss National Science Foundation [grant numbers 200020_169122 / 1]; and the European Research Council under Advanced Grant (INTICE) [grant number 669908].

Data Availability

Data is at the ETHZ repository and can be provided upon request.

Data Statement

Due to the fact that all the collected data are displayed in the final form of various graphs, the data are not presented separately.

Appendix

Bitumen is a complex material with temperature-dependent viscoelastic mechanical properties. Figure A1a shows plots of the complex modulus of bitumen vs. frequency using a dynamic shear rheometer (DSR; Physica MCR 301 DSR, Anton Paar® GmbH, Austria). The bitumen that was used was virgin Q8 70/100 bitumen, and the frequency sweep was done from 0.1 to 20 Hz for temperatures of -10 °C, 0 °C, 10 °C, 20 °C, 30 °C (Figure A1b).

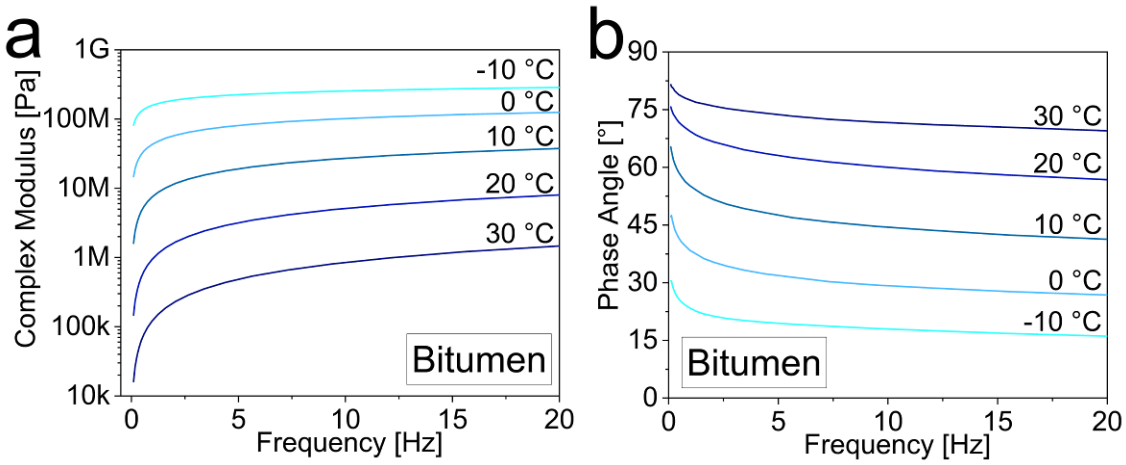

Figure A1 **Dynamic shear rheometer results of bitumen over frequency sweep at different temperatures.** a) Complex modulus vs. frequency of for various temperatures. b) Phase angle vs. frequency for various temperatures.

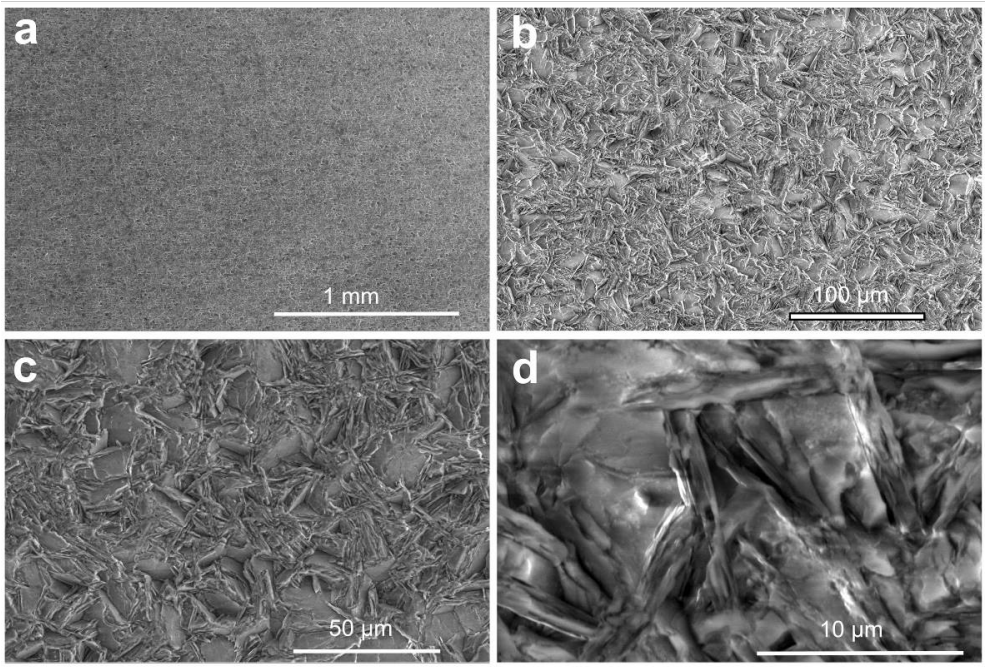

449

450 Figure A2 **Surface topography of Macor®.** a)-d) SEM micrographs of the untreated
451 Macor® surface used in the study. Magnification increases from (a) to (d).

452

453 Figure A2 shows that the surface roughness features are in the microscale range. Figure A3
454 shows an example surface topography of Macor® measured by a profilometer, and we found that
455 the root-mean-square (RMS) surface roughness was 0.34 ± 0.04 µm (average of five separate
456 measurements).

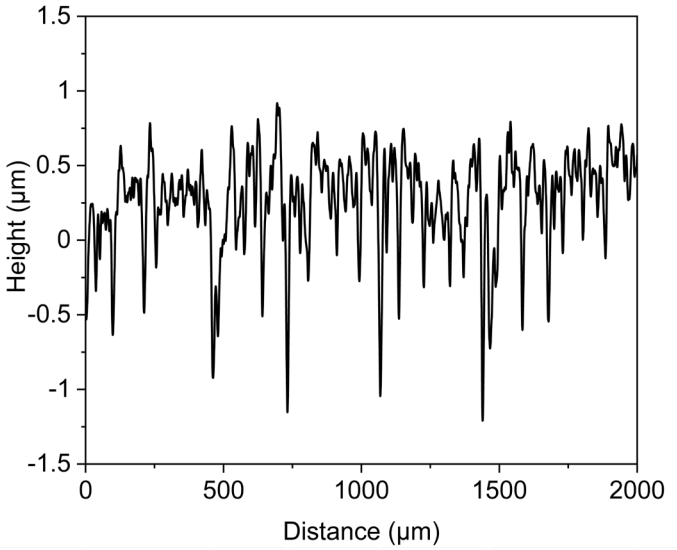

Figure A3 **Surface roughness of Macor®.** A single linear profilometry scan of the untreated Macor® surface used in this study. We did five separate linear scans that were 2 mm long, and we found that the average RMS roughness was 0.34 ± 0.04 µm.

In comparison, X. Gan *et al.* have reported that the RMS surface roughness of aggregates used in pavement is in the range of ~25 µm to ~34 µm (Gan, 2017; see Table A1). For cold regions application, researchers characterized similar aggregates and found that they had RMS surface roughness values of ~6 µm (granite) and ~7 µm (gabbro) (Perez et al., 2015). So while the RMS surface roughness of untreated Macor® is smaller than that of aggregates used in cold regions, we also found that by treating Macor® with a superhydrophobic coating the ice adhesion stress was reduced. Also, if the aggregates are treated to be superhydrophobic, water will not penetrate through the surface for the larger roughnesses typical of the aggregates mentioned above. Hence, in this case the effect of roughness on adhesion is expected to be minor.

Table A1 Comparison of surface roughness from various aggregates and Macor ®.

Rock type	Macor ®	Granite	Gabbro	Limestone	Basalt
	0.34 ± 0.04	29.00 (Gan, 2017)	33.87 (Gan, 2017)	32.06 (Gan, 2017)	24.84 (Gan, 2017)

RMS roughness [µm] (ref.)		6.35±0.90 (Perez et al., 2015)	7.21±0.67 (Perez et al., 2015)		

As it is not possible to cut the Macor® substrate, we cast bitumen on the same geometry glass coverslip. Cross-section of solvent cast bitumen on circular 18 mm diameter glass coverslip shows uniform thickness far away from the sample edge. Here we show cross-section images of a bitumen coating with a thickness of ca. 225 µm on a glass coverslip (Figure A4a) and superhydrophobic coated circular 18 mm diameter Macor® with a coating thickness of ca. 25 µm (Figure A4b).

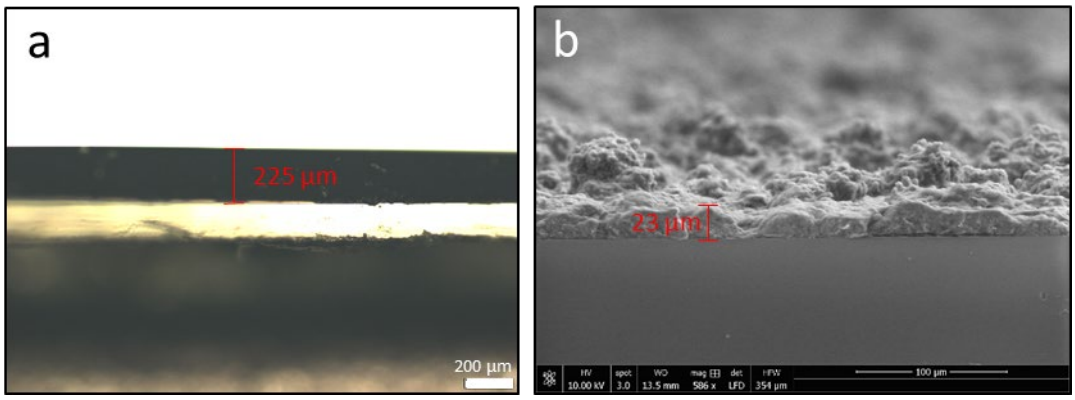

Figure A4 **Thickness analysis of bitumen and superhydrophobic coating.** a) Cross-sectional image of a bitumen coating on glass coverslip revealing its thickness. b) Scanning electron micrograph showing a view of a superhydrophobic coating Macor®.

Figure A5 depicts the contact angle measurement setup. A homemade environmental chamber equipped with a thermoelectric temperature stage and inlet nitrogen to keep environmental condition dry (RH < 1%) at 24 ± 1 °C. The homemade chamber is installed on a commercial goniometer apparatus (OCA35, DataPhysics Instruments GmbH) which only the camera, syringe, and light source are shown in Figure A5.

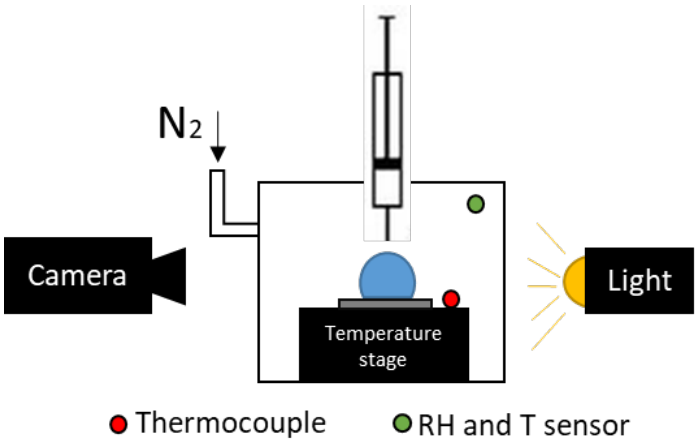

Figure A5 **Contact angle measurement setup.** Schematic drawing of an environmental chamber with nitrogen inlet to control *RH* and thermoelectric modulus installed as temperature stage to control the sample temperature. Green dot shows the location of the environmental temperature and *RH* and red dot shows the location of a thermocouple attached to the stage to measure the sample temperature. The environmental chamber is installed on a commercial goniometer apparatus which camera, syringe, and light source are belonged.

Custom build ice adhesion setup is shown in Figure A6a, b. It consists of four main sections: 1-cryogenic stage, liquid nitrogen reservoir, and its controller, 2- transparent environmental chamber with inlet N_2 to provide the dry experimental ambient condition, 3- Mark-10 model M5-5 force sensor connected to a rod to apply/record force. 4- NRT150/M linear stage from Thorlabs for constant velocity movements of the force sensor.

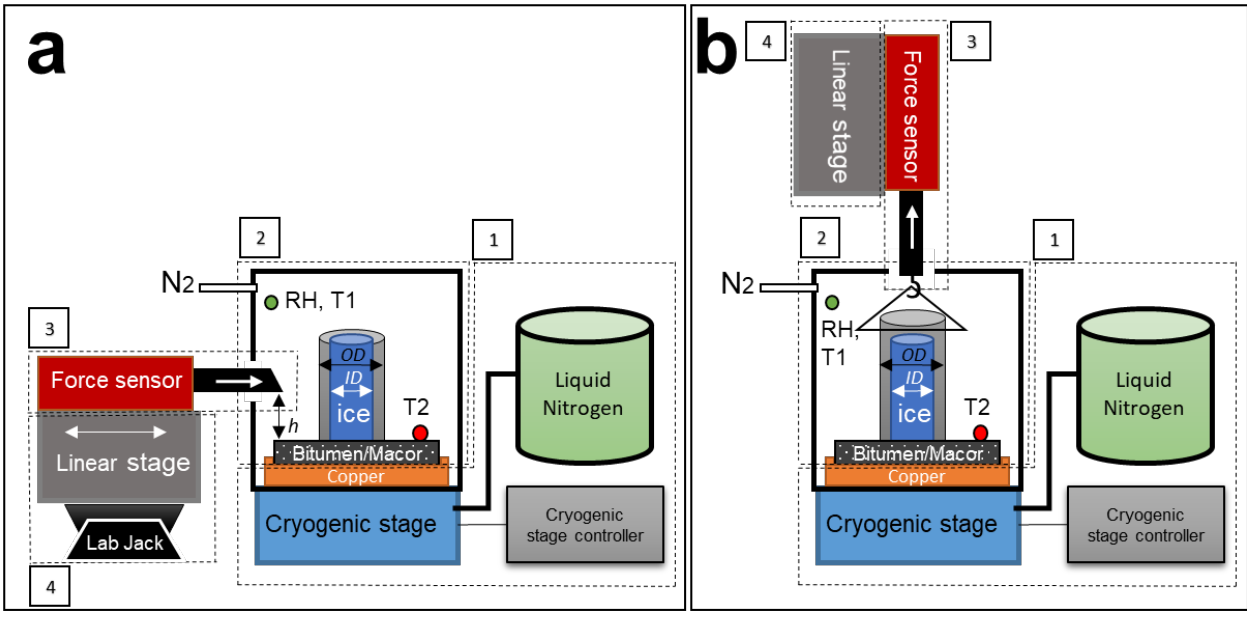

Figure A6 **Schematic drawing of the ice adhesion experimental setup.** a) For pure shear and combined stresses experiments, b) for normal-tension stress experiments. The cryogenic stage setup controls temperature (1), the chamber keeps the environmental *RH* < 1% condition in control, the green dot shows the location of the environmental temperature (T1) and *RH* sensor, and the red dot shows the location of a T-type thermocouple which reads the sample surface temperature. (2), the force sensor measures and records the force (3). The linear stage provides constant velocity to apply force for ice adhesion measurements (4) and lab jack to change the applied force height *h* for pure shear and combined stresses experiments.

To form ice, a water column (volume ~25 µl) was gently placed on the test surface, which is then cooled down to -20 °C. Figure A7b shows the water column on the bitumen surface. Figure A7c shows the water column freezing, and Figure A7d shows it after it has completely frozen. We see that ice nucleation starts from the liquid-substrate interface and propagates upwards. After several minutes, the entire column freezes. Figure A7d shows that the ice is cloudy, which we attribute to small bubbles that form naturally during freezing. We note that we did not detect any large, trapped air pockets.

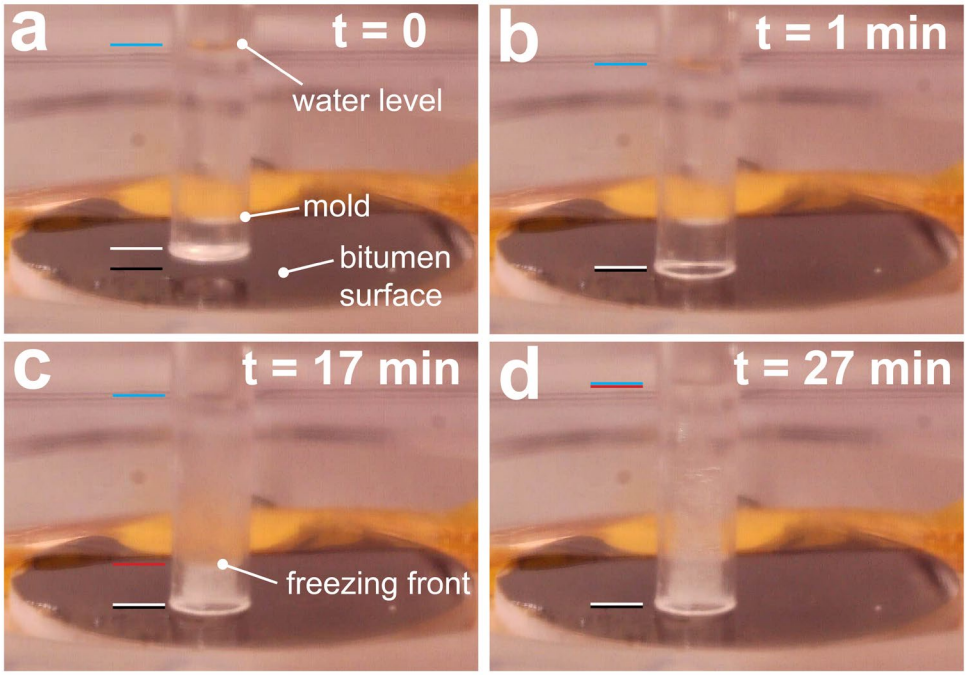

Figure A7 **Forming ice for ice adhesion experiments**. a) The mold is filled with water and is placed in contact with bitumen. Lines shown: bitumen surface (—), bottom of water mold (white line) and the water level (—). b) The water column is placed in contact with the bitumen surface. c) The substrate is cooled and the water starts to freeze (opaque). The freezing front propagates upwards from the bottom (—). d) The water column is completely frozen and is opaque, indicating the presence of tiny bubbles.

Figure A8a shows top-view schematics of ice mold on composite samples in two parallel and perpendicular directions to the applied force. For studying the impact of the material order, the ice mold was placed on the boundary of rigid-soft materials where the notch size is 1.8 mm (Figure A8b). We repeated the material order experiments on superhydrophobic coated Macor® samples.

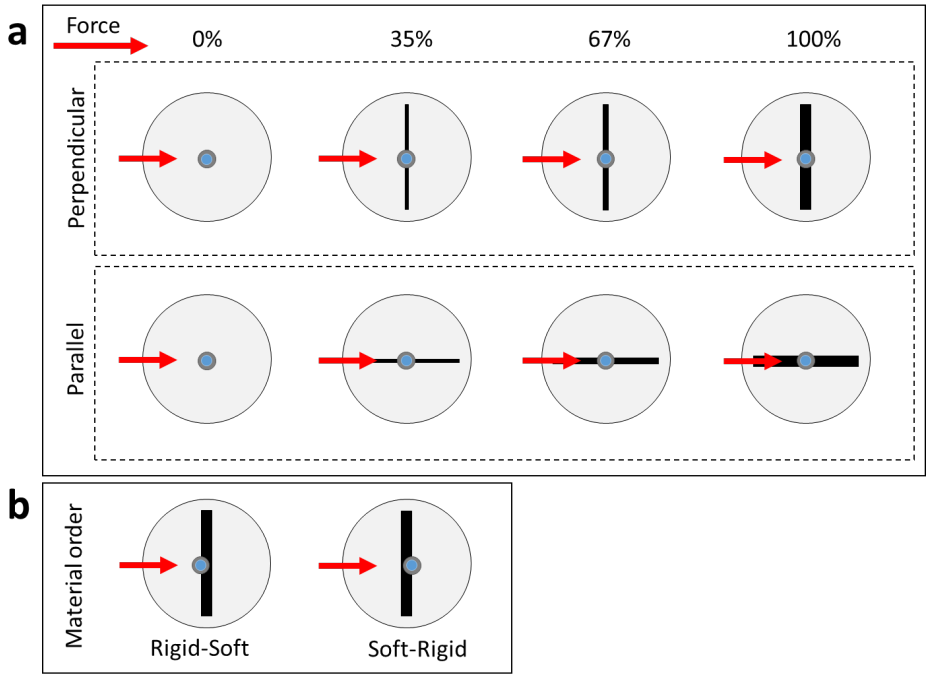

Figure A8 **Bitumen stripe and applied force directions for ice adhesion measurements on bituminous substrates.** a) Sample direction for two directions of the bitumen stripe when is perpendicular or parallel with respect to the applied force. Schematics show bitumen stripe width at three area fraction percentages ϕ regarding 35%, 67%, and 100% of iced area coverage. b) Schematic drawing of placing samples on the boundaries of 1.8 mm bitumen stripe with Macor®, when Macro® is first material with respect to the applied force or the opposite.

References

Ahammed, M., Tighe, S.L., 2009. Early-life, long-term, and seasonal variations in skid resistance in flexible and rigid pavements. Transp. Res. Rec. 112–120. https://doi.org/10.3141/2094-12

Arabzadeh, A., Ceylan, H., Kim, S., Gopalakrishnan, K., Sassani, A., 2016. Superhydrophobic Coatings on Asphalt Concrete Surfaces. Transp. Res. Rec. J. Transp. Res. Board 2551, 10–17. https://doi.org/10.3141/2551-02

Arabzadeh, A., Ceylan, H., Kim, S., Gopalakrishnan, K., Sassani, A., Sundararajan, S., Taylor, P.C., 2017. Superhydrophobic coatings on Portland cement concrete surfaces. Constr. Build. Mater. 141, 393–401. https://doi.org/10.1016/j.conbuildmat.2017.03.012

Baker, H.R., Bascom, W.D., Singleterry, C.R., 1962. The adhesion of ice to lubricated surfaces. J. Colloid Sci. 17, 477–491. https://doi.org/10.1016/0095-8522(62)90057-0

Beemer, D.L., Wang, W., Kota, A.K., 2016. Durable gels with ultra-low adhesion to ice. J. Mater. Chem. A 4, 18253–18258. https://doi.org/10.1039/c6ta07262c

Carré, A., Gastel, J.-C., Shanahan, M.E.R., 1996. Viscoelastic effects in the spreading of liquids. Nature 379, 432–434. https://doi.org/10.1038/379432a0

Chaudhury, M.K., Kim, K.H., 2007. Shear-induced adhesive failure of a rigid slab in contact with a thin confined film. Eur. Phys. J. E 23, 175–183. https://doi.org/10.1140/epje/i2007-10171-x

Chen, H., Wu, Y., Xia, H., Jing, B., Zhang, Q., 2018a. Review of ice-pavement adhesion study and development of hydrophobic surface in pavement deicing. J. Traffic Transp. Eng. (English Ed.). https://doi.org/10.1016/j.jtte.2018.03.002

557 Chen, H., Wu, Y., Xia, H., Zhang, Z., Yuan, T., 2018b. Anti-freezing asphalt concrete: ice-adhesion
558 performance. J. Mater. Sci. 53, 4781–4795. https://doi.org/10.1007/s10853-017-1866-z

559 Chung, J.Y., Chaudhury, M.K., 2005. Soft and Hard Adhesion. J. Adhes. 81, 1119–1145.
560 https://doi.org/10.1080/00218460500310887

561 Chung, J.Y., Kim, K.H., Chaudhury, M.K., Sarkar, J., Sharma, A., 2006. Confinement-induced
562 instability and adhesive failure between dissimilar thin elastic films. Eur. Phys. J. E 20, 47–53.
563 https://doi.org/10.1140/epje/i2005-10080-0

564 Dan, H.C., He, L.H., Zou, J.F., Zhao, L.H., Bai, S.Y., 2014. Laboratory study on the adhesive
565 properties of ice to the asphalt pavement of highway. Cold Reg. Sci. Technol. 104–105, 7–
566 13. https://doi.org/10.1016/j.coldregions.2014.04.002

567 Fischer, H.R., Dillingh, E.C., Hermse, C.G.M., 2014. On the microstructure of bituminous binders.
568 Road Mater. Pavement Des. 15, 1–15. https://doi.org/10.1080/14680629.2013.837838

569 Gan, X., 2017. Measurement and Characterization of Aggregate Surface Texture 100, 421–426.
570 https://doi.org/10.2991/icmeim-17.2017.71

571 Gao, Y., Qu, L., He, B., Dai, K., Fang, Z., Zhu, R., 2018. Study on effectiveness of anti-icing and
572 deicing performance of super-hydrophobic asphalt concrete. Constr. Build. Mater. 191, 270–
573 280. https://doi.org/10.1016/j.conbuildmat.2018.10.009

574 Gerber, J., Lendenmann, T., Eghlidi, H., Schutzius, T.M., Poulikakos, D., 2019. Wetting transitions
575 in droplet drying on soft materials. Nat. Commun. 10, 4776. https://doi.org/10.1038/s41467-
576 019-12093-w

577 Golovin, K., Dhyani, A., Thouless, M.D., Tuteja, A., 2019. Low–interfacial toughness materials for
578 effective large-scale deicing. Science (80-.). 364, 371–375.
579 https://doi.org/10.1126/science.aav1266

580 Irajizad, P., Al-Bayati, A., Eslami, B., Shafquat, T., Nazari, M., Jafari, P., Kashyap, V., Masoudi, A.,
581 Araya, D., Ghasemi, H., 2019a. Stress-localized durable icephobic surfaces. Mater. Horizons
582 6, 758–766. https://doi.org/10.1039/c8mh01291a

583 Irajizad, P., Nazifi, S., Ghasemi, H., 2019b. Icephobic surfaces: Definition and figures of merit. Adv.
584 Colloid Interface Sci. 269, 203–218. https://doi.org/10.1016/j.cis.2019.04.005

585 Kendall, K., 1971. The adhesion and surface energy of elastic solids. J. Phys. D. Appl. Phys. 4, 320.
586 https://doi.org/10.1088/0022-3727/4/8/320

587 Kim, P., Wong, T.S., Alvarenga, J., Kreder, M.J., Adorno-Martinez, W.E., Aizenberg, J., 2012. Liquid-
588 infused nanostructured surfaces with extreme anti-ice and anti-frost performance. ACS
589 Nano 6, 6569–6577. https://doi.org/10.1021/nn302310q

590 Kogbara, R.B., Masad, E.A., Kassem, E., Scarpas, A., Anupam, K., 2016. A state-of-the-art review
591 of parameters influencing measurement and modeling of skid resistance of asphalt
592 pavements. Constr. Build. Mater. 114, 602–617.
593 https://doi.org/10.1016/j.conbuildmat.2016.04.002

594 Kulinich, S.A., Farzaneh, M., 2009. How wetting hysteresis influences ice adhesion strength on
595 superhydrophobic surfaces. Langmuir 25, 8854–8856. https://doi.org/10.1021/la901439c

596 Lee, J.B., dos Santos, S., Antonini, C., 2016. Water Touch-and-Bounce from a Soft Viscoelastic

Substrate: Wetting, Dewetting, and Rebound on Bitumen. Langmuir 32, 8245–8254. https://doi.org/10.1021/acs.langmuir.6b01796

Liu, J., Zhu, C., Liu, K., Jiang, Y., Song, Y., Francisco, J.S., Zeng, X.C., Wang, J., 2017. Distinct ice patterns on solid surfaces with various wettabilities. Proc. Natl. Acad. Sci. U. S. A. 114, 11285–11290. https://doi.org/10.1073/pnas.1712829114

MACOR® Machinable Glass Ceramic For Industrial Applications [WWW Document], 2021. URL https://www.corning.com/worldwide/en/products/advanced-optics/product-materials/specialty-glass-and-glass-ceramics/glass-ceramics/macor.html (accessed 3.15.21).

Matsumoto, K., Kobayashi, T., 2007. Fundamental study on adhesion of ice to cooling solid surface. Int. J. Refrig. 30, 851–860. https://doi.org/10.1016/j.ijrefrig.2006.11.009

Metya, A.K., Singh, J.K., 2019. Ice adhesion mechanism on lubricant-impregnated surfaces using molecular dynamics simulations. Mol. Simul. 45, 394–402. https://doi.org/10.1080/08927022.2018.1513649

Meuler, A.J., Smith, J.D., Varanasi, K.K., Mabry, J.M., McKinley, G.H., Cohen, R.E., 2010. Relationships between Water Wettability and Ice Adhesion. ACS Appl. Mater. Interfaces 2, 3100–3110. https://doi.org/10.1021/am1006035

Mitridis, E., Lambley, H., Tröber, S., Schutzius, T.M., Poulikakos, D., 2020. Transparent Photothermal Metasurfaces Amplifying Superhydrophobicity by Absorbing Sunlight. ACS Nano 14, 11712–11721. https://doi.org/10.1021/acsnano.0c04365

Peng, C., Chen, P., You, Z., Lv, S., Xu, F., Zhang, W., Yu, J., Zhang, H., 2018. The anti-icing and mechanical properties of a superhydrophobic coating on asphalt pavement. Constr. Build. Mater. 190, 83–94. https://doi.org/10.1016/j.conbuildmat.2018.09.128

Penn, L.S., Meyerson, A., 1992. Ice-Pavement Bond Prevention: Fundamental Study. Washington, DC.

Perez, A.P., Wåhlin, J., Klein-Paste, A., 2015. Effect of surface roughness and chemistry on ice bonding to asphalt aggregates. Cold Reg. Sci. Technol. 120, 108–114. https://doi.org/10.1016/j.coldregions.2015.08.015

Petit, J., Bonaccurso, E., 2014. General frost growth mechanism on solid substrates with different stiffness. Langmuir 30, 1160–1168. https://doi.org/10.1021/la404084m

Rønneberg, S., Xiao, S., He, J., Zhang, Z., 2020. Nanoscale Correlations of Ice Adhesion Strength and Water Contact Angle. Coatings 10, 379. https://doi.org/10.3390/coatings10040379

Schutzius, T.M., Bayer, I.S., Tiwari, M.K., Megaridis, C.M., 2011. Novel fluoropolymer blends for the fabrication of sprayable multifunctional superhydrophobic nanostructured composites. Ind. Eng. Chem. Res. 50, 11117–11123. https://doi.org/10.1021/ie200814r

Schutzius, T.M., Jung, S., Maitra, T., Eberle, P., Antonini, C., Stamatopoulos, C., Poulikakos, D., 2015. Physics of Icing and Rational Design of Surfaces with Extraordinary Icephobicity. Langmuir 31, 4807–4821. https://doi.org/10.1021/la502586a

Shen, Y., Tao, J., Tao, H., Chen, S., Pan, L., Wang, T., 2015. Superhydrophobic Ti6Al4V surfaces with regular array patterns for anti-icing applications. RSC Adv. 5, 32813–32818.

https://doi.org/10.1039/c5ra01365h

Sivakumar, G., Jackson, J., Ceylan, H., Sundararajan, S., 2021. An investigation on ice adhesion and wear of surfaces with differential stiffness. Wear 203662. https://doi.org/10.1016/j.wear.2021.203662

Soenen, H., Besamusca, J., Fischer, H.R., Poulikakos, L.D., Planche, J.-P., Das, P.K., Kringos, N., Grenfell, J.R.A., Lu, X., Chailleux, E., 2014. Laboratory investigation of bitumen based on round robin DSC and AFM tests. Mater. Struct. 47, 1205–1220. https://doi.org/10.1617/s11527-013-0123-4

Tarpoudi Baheri, F., Schutzius, T.M., Poulikakos, D., Poulikakos, L.D., 2020. Bitumen surface microstructure evolution in subzero environments. J. Microsc. 279, 3–15. https://doi.org/10.1111/jmi.12890

Vasileiou, T., Schutzius, T.M., Poulikakos, D., 2017. Imparting Icephobicity with Substrate Flexibility. Langmuir 33, 6708–6718. https://doi.org/10.1021/acs.langmuir.7b01412

Wang, C., Fuller, T., Zhang, W., Wynne, K.J., 2014. Thickness dependence of ice removal stress for a polydimethylsiloxane nanocomposite: Sylgard 184. Langmuir 30, 12819–12826. https://doi.org/10.1021/la5030444

Wang, C., Gupta, M.C., Yeong, Y.H., Wynne, K.J., 2018. Factors affecting the adhesion of ice to polymer substrates. J. Appl. Polym. Sci. 135, 45734. https://doi.org/10.1002/app.45734

Wang, N., Tang, L., Tong, W., Xiong, D., 2018. Fabrication of robust and scalable superhydrophobic surfaces and investigation of their anti-icing properties. Mater. Des. 156, 320–328.

https://doi.org/10.1016/j.matdes.2018.06.053

Wilson, P.W., Lu, W., Xu, H., Kim, P., Kreder, M.J., Alvarenga, J., Aizenberg, J., 2013. Inhibition of ice nucleation by slippery liquid-infused porous surfaces (SLIPS). Phys. Chem. Chem. Phys. 15, 581–585. https://doi.org/10.1039/c2cp43586a

Work, A., Lian, Y., 2018. A critical review of the measurement of ice adhesion to solid substrates. Prog. Aerosp. Sci. 98, 1–26. https://doi.org/10.1016/j.paerosci.2018.03.001

Xia, H., Zhao, X., Wu, Y., Yuan, T., Song, L., Yan, M., Wang, F., Chen, H., 2020. Preparation and performance of antifreeze adhesive materials for asphalt pavement. Constr. Build. Mater. 258. https://doi.org/10.1016/j.conbuildmat.2020.119554

Yu, X., Burnham, N.A., Tao, M., 2015. Surface microstructure of bitumen characterized by atomic force microscopy. Adv. Colloid Interface Sci. 218, 17–33. https://doi.org/10.1016/j.cis.2015.01.003